

See discussions, stats, and author profiles for this publication at: <https://www.researchgate.net/publication/6559024>

# Bonding and Electronic Structure of XeF<sub>3</sub> –

ARTICLE in JOURNAL OF THE AMERICAN CHEMICAL SOCIETY · FEBRUARY 2007

Impact Factor: 12.11 · DOI: 10.1021/ja065038b · Source: PubMed

CITATIONS

19

READS

485

6 AUTHORS, INCLUDING:



Changtong Hao

Advion

21 PUBLICATIONS 169 CITATIONS

SEE PROFILE



Catherine Check

Northern Illinois University

23 PUBLICATIONS 683 CITATIONS

SEE PROFILE



Lee S Sunderlin

Northern Illinois University

68 PUBLICATIONS 2,544 CITATIONS

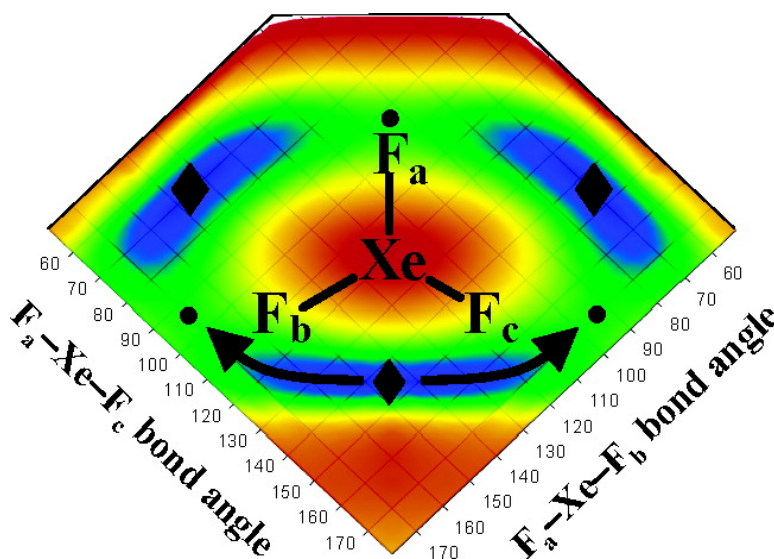
SEE PROFILE

## Bonding and Electronic Structure of XeF

Ian H. Krouse, Changtong Hao, Catherine E. Check, Kim C. Lobring, Lee S. Sunderlin, and Paul G. Wenthold

*J. Am. Chem. Soc.*, **2007**, 129 (4), 846-852 • DOI: 10.1021/ja065038b • Publication Date (Web): 03 January 2007

Downloaded from <http://pubs.acs.org> on May 13, 2009



### More About This Article

Additional resources and features associated with this article are available within the HTML version:

- Supporting Information
- Links to the 4 articles that cite this article, as of the time of this article download
- Access to high resolution figures
- Links to articles and content related to this article
- Copyright permission to reproduce figures and/or text from this article

[View the Full Text HTML](#)



**ACS Publications**  
High quality. High impact.

Bonding and Electronic Structure of  $\text{XeF}_3^-$ Ian H. Krouse,<sup>†,‡</sup> Changtong Hao,<sup>§</sup> Catherine E. Check,<sup>§,#</sup> Kim C. Lobring,<sup>§</sup>  
Lee S. Sunderlin,<sup>\*,§</sup> and Paul G. Wenthold<sup>\*,†</sup>*Contribution from the Department of Chemistry and Biochemistry, Northern Illinois University,  
DeKalb, Illinois 60115, and Department of Chemistry, Purdue University,  
West Lafayette, Indiana 47907*

Received July 14, 2006; E-mail: sunder@niu.edu; pgw@purdue.edu

**Abstract:** The xenon–fluoride bond dissociation energy in  $\text{XeF}_3^-$  has been measured by using energy-resolved collision-induced dissociation studies of the ion. The measured value,  $0.84 \pm 0.06$  eV, is higher than that predicted by electrostatic and three-center, four-electron bonding models. The bonding in  $\text{XeF}_3^-$  is qualitatively described by using molecular orbital approaches, using either a diradical approach or orbital interaction models. Two low-energy singlet structures are identified for  $\text{XeF}_3^-$ , consisting of Y- and T-shaped geometries, and there is a higher energy  $D_{3h}$  triplet state. Electronic structure calculations predict the Y geometry to be the lowest energy structure, which can rearrange by pseudorotation through the T geometry. Orbital correlation diagrams indicate that that ion dissociates by first rearranging to the T structure before losing fluoride.

The combination of xenon with other elements through chemical means presents a scientific challenge. In 1962, Bartlett<sup>1</sup> reported the first evidence of a xenon-containing compound, and shortly after compounds such as  $\text{XeF}_2$ ,<sup>2</sup>  $\text{XeF}_4$ ,<sup>3</sup>  $\text{XeF}_6$ , and  $\text{XeOF}_4$ <sup>4</sup> were described. Until 1980, the only stable xenon-containing compounds generally had xenon bonded to F or O, although the carbon-bonded species  $\text{CH}_3\text{Xe}^+$  had been detected by using ion cyclotron resonance mass spectrometry.<sup>5,6</sup> The landscape changed in the early 1980s, when several xenon–nitrogen bonded species were reported.<sup>7–9</sup> Many types of xenon-containing compounds are now fairly common, and some, such as xenon difluoride, are commercially available. Because of this availability, the physical properties and reactivity of xenon-containing species are becoming better understood.<sup>10–13</sup> For example, xenon difluoride is known to be a strong Lewis acid,<sup>14</sup> and its Lewis acidity has been studied in both the solid and solution phases. Thus, molecules with highly electronegative

atoms such as O, N, and S<sup>15</sup> and even activated carbon-based ligands<sup>16</sup> bond with xenon.

Although much of the previous work has involved the characterization of  $\text{XeF}^+$  reagents in the condensed phase, some gas-phase studies have been performed. Both positive<sup>17–19</sup> and negative<sup>20,21</sup> ion mass spectrometry of  $\text{XeF}_2$  has been reported. Positive ion electron ionization (EI) of  $\text{XeF}_2$  produces  $\text{XeF}_2^+$ ,  $\text{XeF}^+$ , and  $\text{Xe}^+$ , whereas negative ion EI leads to  $\text{XeF}_3^-$ ,  $\text{XeF}_2^-$ ,  $\text{XeF}^-$ ,  $\text{F}_2^-$ , and  $\text{F}^-$ . Negative ion EI mass spectrometry of  $\text{XeF}_6$  has shown that stepwise losses of F and  $\text{F}_2$  occur, giving anionic products  $\text{XeF}^-$ ,  $\text{XeF}_2^-$ ,  $\text{XeF}_3^-$ ,  $\text{XeF}_4^-$ ,  $\text{F}_2^-$ , and  $\text{F}^-$ ,<sup>20</sup> and the negative ion EI mass spectra of  $\text{XeOF}_4$  and  $\text{XeF}_4$  have also been reported.<sup>20</sup> In general, little is known about the bonding in xenon-containing anionic species. One representative example of such a species in the condensed phase is the pentagonal planar  $\text{XeF}_5^-$  crystallized as  $[\text{N}(\text{CH}_3)_4^+][\text{XeF}_5^-]$ ,<sup>22</sup> which was characterized by using X-ray crystallography, <sup>19</sup>F/<sup>129</sup>Xe NMR, and Raman/IR spectroscopy. Dixon and co-workers<sup>23</sup> have recently reported extensive high-level calculations on the structures and thermochemical properties of the known xenon fluorides and xenon fluoride ions, including  $\text{XeF}^-$ ,  $\text{XeF}_2^-$ ,  $\text{XeF}_4^-$ ,  $\text{XeF}_5^-$ , and  $\text{XeF}_6^-$ .

<sup>†</sup> Purdue University.<sup>§</sup> Northern Illinois University.<sup>‡</sup> Present address: Department of Chemistry & Biochemistry, Denison University, Granville, OH 43023.<sup>#</sup> Present address: Department of Sciences, Rock Valley College, Rockford, IL 61114.

- (1) Bartlett, N. *Proc. Chem. Soc., London* **1962**, 218.
- (2) Hoppe, R.; Mattauch, H.; Roedder, K. M.; Martin, K.; Daehne, W. Z. *Anorg. Allg. Chem.* **1963**, 323, 214.
- (3) Classen, H. H.; Selig, H.; Malm, J. G. *J. Am. Chem. Soc.* **1962**, 84, 3593.
- (4) Malm, J. G.; Sheft, I.; Chernick, C. L. *J. Am. Chem. Soc.* **1963**, 85, 110.
- (5) Holtz, D.; Beauchamp, J. L. *Science* **1971**, 173, 1237.
- (6) Hovey, J. K.; McMahon, T. B. *J. Am. Chem. Soc.* **1986**, 108, 528.
- (7) Schumacher, G. A.; Schrobilgen, G. J. *Inorg. Chem.* **1983**, 22, 2178.
- (8) DesMarteau, D. D.; LeBlond, R. D.; Hossian, S. F.; Nothe, D. *J. Am. Chem. Soc.* **1981**, 103, 7734.
- (9) Sawyer, J. F.; Schrobilgen, G. J. *Inorg. Chem.* **1983**, 21, 4064.
- (10) Bartlett, N.; Sladky, F. O. The Chemistry of Krypton, Xenon, and Radon. In *Comprehensive Inorganic Chemistry*; Trotman-Dickenson, A. F., Ed.; Pergamon Press: Oxford, 1973; Vol. 1, pp 213.
- (11) Seppelt, K.; Lentz, D. *Prog. Inorg. Chem.* **1982**, 29, 167.
- (12) Moody, G. J. *J. Chem. Educ.* **1974**, 51, 628.
- (13) Christe, K. O. *Angew. Chem., Int. Ed.* **2001**, 40, 1419.

- (14) Schrobilgen, G. J. *Synth. Fluorine Chem.* **1992**, 1.
- (15) Pettersson, M.; Lundell, J.; Khriachtchev, L.; Isoniemi, E.; Räsänen, M. *J. Am. Chem. Soc.* **1998**, 120, 7979.
- (16) Frohn, H.-J.; Bardin, V. V. *Organometallics* **2001**, 20, 4750.
- (17) Morrison, J. D.; Nicholson, A. J. C.; O'Donnell, T. A. *J. Chem. Phys.* **1968**, 49, 959.
- (18) Berkowitz, J.; Chupka, W. A.; Guyon, P. M.; Holloway, J. H.; Spohr, R. *J. Phys. Chem.* **1971**, 75, 1461.
- (19) Krouse, I. H.; Wenthold, P. G. *Inorg. Chem.* **2003**, 42, 4293.
- (20) Begun, G. M.; Compton, R. N. *J. Chem. Phys.* **1969**, 51, 2367.
- (21) Begun, G. M.; Compton, R. N. *Int. J. Mass Spectrom. Ion Phys.* **1979**, 30, 379.
- (22) Christe, K. O.; Curtis, E. C.; Dixon, D. A.; Mercier, H. P.; Sanders, J. C. P.; Schrobilgen, G. J. *J. Am. Chem. Soc.* **1991**, 113, 3351.
- (23) Dixon, D. A.; deJong, W. A.; Peterson, K. A.; Christe, K. O.; Schrobilgen, G. J. *J. Am. Chem. Soc.* **2005**, 127, 8627.

In conjunction with our recent studies of main group fluorides,<sup>19,24–26</sup> we have examined the properties and gas-phase reactivity of xenon-containing ions. In this work, we describe an investigation of  $\text{XeF}_3^-$ , formed by addition of fluoride to  $\text{XeF}_2$ . Although the ion has not been observed in the condensed phase,<sup>27</sup> it has been reported previously as a mass spectrometric product formed upon ionization of  $\text{XeF}_2$ ,  $\text{XeF}_4$ , and  $\text{XeF}_6$ .<sup>20,21</sup> By using energy-resolved mass spectrometry of  $\text{XeF}_3^-$ , we have determined the fluoride affinity of  $\text{XeF}_2$ . On the basis of the experimental data and electronic structure calculations, we provide molecular orbital descriptions of the bonding in and dissociation of the hypervalent ion.

## Experimental Section

The bond dissociation energy in  $\text{XeF}_3^-$  was measured using the energy-resolved collision-induced dissociation (CID) technique<sup>28,29</sup> in a flowing afterglow tandem mass spectrometer (MS).<sup>30</sup> The instrument consists of an ion source region, a flow tube, and the tandem MS. The DC discharge ion source used in these experiments is typically set at 2000 V, with 2 mA of emission current. The flow tube is a 92 cm  $\times$  7.3 cm i.d. stainless steel pipe that operates at a buffer gas pressure of 0.35 Torr, a flow rate of 200 standard  $\text{cm}^3 \text{ s}^{-1}$ , and an ion residence time of 10 ms. The buffer gas is helium with up to 10% argon added to stabilize the DC discharge.

To make  $\text{XeF}_3^-$  for this study,  $\text{XeF}_2$  was added to the ion source. Dissociative electron impact gave  $\text{F}^-$ , which undergoes ternary addition to the  $\text{XeF}_2$  molecule in the presence of helium to make the desired ion.  $\text{XeF}_2$  was cooled in an ice bath to improve control of the vapor flow. Approximately  $10^5$  collisions with the buffer gas cool the metastable ions to room temperature.

The tandem MS includes a quadrupole mass filter, an octopole ion guide, a second quadrupole mass filter, and a detector, contained in a stainless steel box that is partitioned into five interior chambers with differential pumping to minimize collisions with background gases. During CID experiments, the ions are extracted from the flow tube and focused into the first quadrupole for mass selection. The reactant ions are then focused into the octopole, which passes through a reaction cell that contains an argon collision gas. Use of argon collision gas gives more precision for the relatively weakly bound  $\text{XeF}_3^-$  anion and avoids potential fluorine/fluoride transfer reactions between the two Xe atoms. After the dissociated and unreacted ions pass through the reaction cell, the second quadrupole is used for mass analysis. The detector is an electron multiplier operating in pulse-counting mode.

The energy threshold for CID is determined by modeling the cross section for product formation as a function of the reactant ion kinetic energy in the center-of-mass (CM) frame,  $E_{\text{cm}}$ . The octopole is used as a retarding field analyzer to measure the reactant ion beam energy zero. The ion kinetic energy distribution for the present data is typically Gaussian, with a full width at half-maximum of 0.8–1.8 eV (1 eV = 96.5 kJ/mol). The octopole offset voltage measured with respect to the center of the Gaussian fit gives the laboratory kinetic energy,  $E_{\text{lab}}$ , in electronvolts. Low offset energies are corrected for truncation of the ion beam.<sup>31,32</sup> To convert to the center-of-mass frame, the equation  $E_{\text{cm}}$

$= E_{\text{lab}}m(m+M)^{-1}$  is used, where  $m$  and  $M$  are the masses of the neutral and ionic reactants, respectively. All experiments were performed with both mass filters at low resolution to improve ion collection efficiency and reduce mass discrimination. Average atomic masses were used for all elements.

The total cross section for a reaction,  $\sigma_{\text{total}}$ , is calculated using eq 1, where  $I$  is the intensity of the reactant ion beam,  $I_0$  is the intensity of the incoming beam ( $I_0 = I + \sum I_i$ ),  $I_i$  is the intensity of each product ion,  $n$  is the number density of the collision gas, and  $l$  is the effective collision length,  $13 \pm 2$  cm. Individual product cross sections  $\sigma_i$  are equal to  $\sigma_{\text{total}} (I_i/\sum I_i)$ .

$$I = I_0 \exp(-\sigma_{\text{total}}nl) \quad (1)$$

Threshold energies are derived by fitting the data to a model function given in eq 2, where  $\sigma(E)$  is the cross section for formation of the product ion at center-of-mass energy  $E$ ,  $E_{\text{T}}$  is the desired threshold energy,  $\sigma_0$  is the scaling factor,  $n$  is an adjustable parameter, and  $i$  denotes rovibrational states having energy  $E_i$  and population  $g_i$  ( $\sum g_i = 1$ ). Doppler broadening and the kinetic energy distribution of the reactant ion are also accounted for in the data analysis, which is done using the CRUNCH program written by Armentrout and co-workers.<sup>31,32</sup>

Collisionally activated metastable complexes can have sufficiently

$$\sigma(E) = \sigma_0 \sum_i P_i g_i (E + E_i - E_{\text{T}})^n/E \quad (2)$$

long lifetimes that they do not dissociate on the experimental time scale (ca. 50  $\mu\text{s}$ ). Such kinetic shifts are accounted for in the CRUNCH program by RRKM lifetime calculations. Reactant and product vibrational frequencies are needed to determine both the RRKM lifetimes and the reactant internal energy distribution.

Experimental vibrational frequency sets are not available for  $\text{XeF}_3^-$ . To give a consistent set of frequencies, therefore, vibrational and rotational frequencies were calculated using the B3LYP model and basis sets discussed below. Uncertainties in the derived thresholds due to possible inaccuracies in the frequencies were estimated by multiplying the entire sets of frequencies by 0.9 and 1.1, and by multiplying the time window for dissociation by 10 and 0.1. The effect of this scaling on the calculated thresholds is 3 kJ  $\text{mol}^{-1}$  for  $\text{XeF}_3^-$ . Final uncertainties are reported as the square root of the sum of the square of the standard deviation of the reaction thresholds for individual data sets, the uncertainty due to fitting parameters, and a 0.15 eV (laboratory) contribution due to uncertainty in the absolute energy scale. Polarizabilities for neutral molecules were also taken from the computational results; varying these parameters has a negligible effect on the derived bond strengths. An ion not sufficiently energized by one collision with the target gas may gain enough energy in a second collision to be above the dissociation threshold. This effect is eliminated by linear extrapolation of the data taken at several pressures to a zero-pressure cross section before fitting the data.<sup>33,34</sup>

$\text{XeF}_2$  was obtained from SynQuest Laboratories (Alachua, FL). He, Ar, and  $\text{SF}_6$  were obtained from BOC,  $\text{F}_2$  was obtained from Air Products, and Xe was obtained from Spectra Gases. All reagents were used as received, except He, which was passed through a drying trap at  $-196^\circ\text{C}$  prior to use.

## Computational Methods

Computational studies of  $\text{XeF}_3^-$  were performed using Gaussian 98 and Gaussian 03.<sup>35,36</sup> All molecular structures were optimized with and without symmetry constraints, and plausible alternative structures were

- (24) Krouse, I. H.; Lardin, H. A.; Wenthold, P. G. *Int. J. Mass Spectrom.* **2003**, 227, 303.
- (25) Artau, A.; Nizzi, K. E.; Hill, B. T.; Sunderlin, L. S.; Wenthold, P. G. *J. Am. Chem. Soc.* **2000**, 122, 10667.
- (26) Krouse, I. H.; Wenthold, P. G. *J. Am. Soc. Mass Spectrom.* **2005**, 16, 697.
- (27) The ion has been proposed as an intermediate in the fluoride exchange reaction of  $\text{XeF}_2$ : Vasdev, N.; Pointner, B. E.; Chirakal, R.; Schrobilgen, G. J. *J. Am. Chem. Soc.* **2002**, 124, 12863.
- (28) Muntean, F.; Armentrout, P. B. *J. Chem. Phys.* **2001**, 115, 1213.
- (29) Armentrout, P. B. *J. Am. Soc. Mass Spectrom.* **2002**, 13, 419.
- (30) Do, K.; Klein, T. P.; Pommerening, C. A.; Sunderlin, L. S. *J. Am. Soc. Mass Spectrom.* **1997**, 8, 688.
- (31) Rodgers, M. T.; Ervin, K. M.; Armentrout, P. B. *J. Chem. Phys.* **1997**, 106, 4499.
- (32) Ervin, K. M.; Armentrout, P. B. *J. Chem. Phys.* **1985**, 83, 166.

- (33) Loh, S. K.; Hales, D. A.; Lian, L.; Armentrout, P. B. *J. Chem. Phys.* **1989**, 90, 5466.
- (34) Schultz, R. H.; Crellin, K. C.; Armentrout, P. B. *J. Am. Chem. Soc.* **1991**, 113, 8590.
- (35) Frisch, M. J.; et al. *Gaussian 98*, Revision A.11.3; Gaussian, Inc.: Pittsburgh, PA, 2002.
- (36) Frisch, M. J.; et al. *Gaussian 03*, Revision B.05; Gaussian, Inc.: Pittsburgh, PA, 2003.

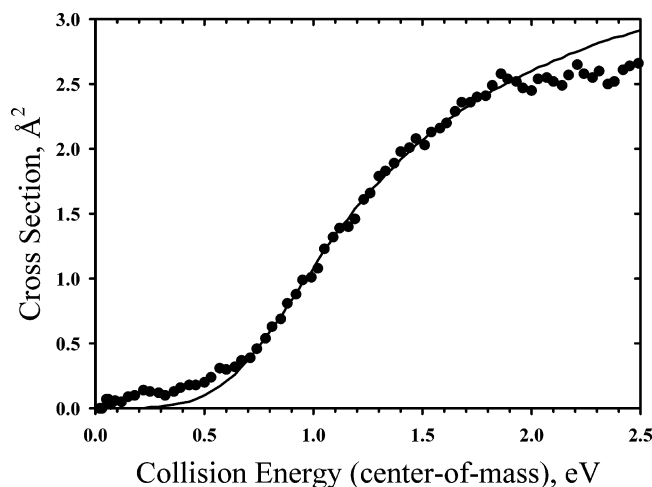


**Figure 1.** Modeled cross-sectional data for the formation of  $F^-$  upon energy-resolved CID of  $XeF_3^-$ . The solid line is the fit to the data, obtained using eq 2, with  $E_T = 0.83 \pm 0.05$  eV and  $n = 0.95 \pm 0.14$ , where the uncertainties correspond to one standard deviation of the data from replicate measurements.

tested. Geometries, energies, and vibrational frequencies for the ionic and neutral species were calculated using the B3LYP and MP2 approaches. Basis sets for Xe include SDB-cc-pVTZ,<sup>37–39</sup> which includes an effective core potential for core electrons, with a cc-pVTZ basis set for the valence electrons, and the basis set described by Maroulis,<sup>40</sup> which includes all electrons. Basis sets for fluorine include 6-31+G\*, aug-cc-pVDZ, and aug-cc-pVTZ.<sup>41–43</sup> Zero-point energy and thermal energy corrections were obtained from calculated frequencies at the specified level of theory, where possible.

## Results

Electron ionization of  $XeF_2$  produces  $F^-$ , which adds to a second molecule of  $XeF_2$  to make the desired  $XeF_3^-$  ion. Collision-induced dissociation of  $XeF_3^-$  results in formation of  $F^-$  as the major product. Very small amounts (<1%) of  $F_2^-$  were also observed at higher energies but are not discussed further. Some signal that appears to correspond to either  $XeF_2^-$  or  $FXeO^-$  was observed. However, it was found that the ratio of  $F^-/(XeF_2^-, FXeO^-)$  increased slowly over time, indicating that the two products do not arise from the same ion. After many hours, the yield of  $XeF_2^-$  or  $FXeO^-$  was negligible, whereas the cross section for  $F^-$  formation did not change significantly, indicating that the minor product originated from an unidentified impurity ion, possibly  $XeF_2^-(H_2O)$  or  $XeF_2OH^-$ . The hydroxylated ion could be formed independently by reaction of  $XeF_2$  with solvated hydroxide ion<sup>44</sup> and undergoes CID by loss of HF to form  $FXeO^-$ . However, because the experiments were carried out using low-resolution settings (to improve signal intensity), it was not possible to determine the identity of the impurity in these experiments.

**Table 1.** Calculated Structural Parameters and Relative Energies for  $XeF_3^-$

method	Xe basis set <sup>a</sup>	F basis set	relative enthalpy <sup>b</sup>	1D bond <sup>c</sup>	2D bond <sup>d</sup>	angle <sup>e</sup>
Y-Shaped ( $C_{2v}$ )						
B3LYP	I	6-31+G*	0.0	2.158	2.217	145.2
	I	6-311+G(3df)	0.0	2.156	2.216	145.3
	I	aug-cc-pVDZ	0.0	2.156	2.217	145.2
	I	aug-cc-pVTZ	0.0	2.153	2.215	145.3
	II	aug-cc-pVTZ	0.0	2.161	2.233	145.1
MP2	I	6-31+G*	0.0	2.144	2.194	145.4
	II	6-31+G*	0.0	2.156	2.213	145.2
frequencies <sup>f</sup>		38, 183, 267, 277, 368, 397				
T-Shaped ( $C_{2v}$ )						
B3LYP	I	6-31+G*	15.0	2.667	2.062	94.0
	I	6-311+G(3df)	14.7	2.661	2.060	94.0
	I	aug-cc-pVDZ	14.6	2.666	2.061	94.0
	I	aug-cc-pVTZ	13.2	2.665	2.052	93.9
	II	aug-cc-pVTZ	14.5	2.681	2.064	94.5
MP2	I	6-31+G*	6.5	2.684	2.040	93.9
	II	6-31+G*	1.7	2.699	2.046	94.1
frequencies <sup>f</sup>		94i, 194, 217, 222, 448, 487				
$D_{3h}$ (Triplet)						
B3LYP	I	6-31+G*	71.9	2.411		
	I	6-311+G(3df)	72.8	2.409		
	I	aug-cc-pVDZ	72.6	2.409		
	I	aug-cc-pVTZ	73.6	2.412		
	II	aug-cc-pVTZ	58.5	2.426		
MP2	I	6-31+G*	112.8 <sup>g</sup>	2.303		
	II	6-31+G*	96.4 <sup>g</sup>	2.311		
frequencies <sup>f</sup>		$2 \times 72, 104, 227, 2 \times 257$				

<sup>a</sup> I, Maroulis basis set;<sup>40</sup> II, SDB-cc-pVTZ basis set. See text for details.

<sup>b</sup> Values in kJ/mol. <sup>c</sup> Length of the unique Xe–F bond in the  $C_{2v}$  structures, and the bond length for the  $D_{3h}$  structure. Values in Å. <sup>d</sup> Lengths of the equivalent Xe–F bonds in the  $C_{2v}$  structures. Values in Å. <sup>e</sup> Angle between the 1D and 2D bonds in the  $C_{2v}$  structures. Values in deg. <sup>f</sup> Harmonic frequencies calculated using the B3LYP approach with the Maroulis basis set for xenon and the aug-cc-pVTZ basis set for fluorine. <sup>g</sup> Zero-point and thermal energy corrections were obtained using B3LYP harmonic frequencies.

Cross sections for  $F^-$  formation upon CID of  $XeF_3^-$  are shown in Figure 1, along with the model fit of the data. The threshold energy is  $0.83 \pm 0.06$  eV. The measured 0 K bond dissociation energy can be combined with calculated vibrational frequencies to give a bond dissociation enthalpy of  $0.84 \pm 0.06$  eV ( $81 \pm 6$  kJ/mol) at 298 K. This value is only slightly less than the average Xe–F bond dissociation enthalpies in  $XeF_2$ ,  $XeF_4$ , and  $XeF_6$ , which are 93.2, 91.2, and 86.2 kJ/mol, respectively.<sup>45</sup> The measured fluoride binding energy in this work can be used to determine  $\Delta H_f(XeF_3^-) = -437 \pm 6$  kJ/mol, by using  $\Delta H_f(XeF_2) = -107 \pm 1$  kJ/mol<sup>45</sup> and  $\Delta H_f(F^-) = -248.8$  kJ/mol.<sup>46</sup>

Structures, frequencies, and energies were calculated for Y- and T-shaped and  $D_{3h}$   $XeF_3^-$  using both the B3LYP and MP2 methods. In these calculations, the Maroulis and SDB-cc-pVTZ basis sets were used for xenon, whereas the basis sets for fluorine were varied. Optimized bond lengths, bond angles, and relative energies calculated at the different levels of theory are listed in Table 1, along with the frequencies obtained when using the B3LYP approach, the Maroulis basis set for xenon, and the

(37) Martin, J. M. L.; Sundermann, A. *J. Chem. Phys.* **2001**, *114*, 3408.

(38) Bergner, A.; Dolg, M.; Kuechle, W.; Stoll, H.; Preuss, H. *Mol. Phys.* **1993**, *80*, 1431.

(39) Check, C. E.; Lobring, K. C.; Keating, P. R.; Gilbert, T. M.; Sunderlin, L. S. *J. Phys. Chem. A* **2003**, *107*, 8961.

(40) Maroulis, G.; Haskopoulos, A.; Xenides, D. *Chem. Phys. Lett.* **2004**, *396*, 59.

(41) Woon, D. E.; Dunning, T. H., Jr. *J. Chem. Phys.* **1993**, *98*, 1358.

(42) Dunning, T. H., Jr. *J. Chem. Phys.* **1989**, *90*, 1007.

(43) Kendall, R. A.; Dunning, T. H., Jr.; Harrison, R. J. *J. Chem. Phys.* **1992**, *96*, 6796.

(44) Krouse, I. H.; Wenthold, P. G. *Organometallics* **2004**, *23*, 2573.

(45) Johnson, G. K.; Malm, J. G.; Hubbard, W. N. *J. Chem. Thermodyn.* **1972**, *4*, 879.

(46) Bartmess, J. E. Negative Ion Energetics Data. In *NIST Chemistry WebBook, NIST Standard Reference Database Number 69*; Mallard, W. G.; Linstrom, P. J., Eds.; National Institute of Standards and Technology: Gaithersburg, MD, June 2005.



**Table 2.** Calculated Xe–F Bond Dissociation Energies (in eV) in  $\text{XeF}_3^-$ 

method	Xe basis set <sup>a</sup>	F basis set	$D(\text{XeF}_2\text{--F}^-)$ , 0 K <sup>b</sup>	$\Delta H(\text{XeF}_2\text{--F}^-)$ , 298 K
B3LYP	I	6-31+G*	1.10	1.11
	I	6-31++G(3df)	1.14	1.15
	I	aug-cc-pVDZ	1.05	1.06
	I	aug-cc-pVTZ	1.02	1.03
	II	aug-cc-pVTZ	1.04	1.05
MP2	I	6-31+G*	0.93	0.94
	II	6-31+G*	0.82	0.83
MP4 <sup>c</sup>	II	6-31+G*	0.93	0.94
exptl			$0.83 \pm 0.05$	$0.84 \pm 0.06$

<sup>a</sup> I, Maroulis basis set;<sup>40</sup> II, SDB-cc-pVTZ basis set. See text for details.

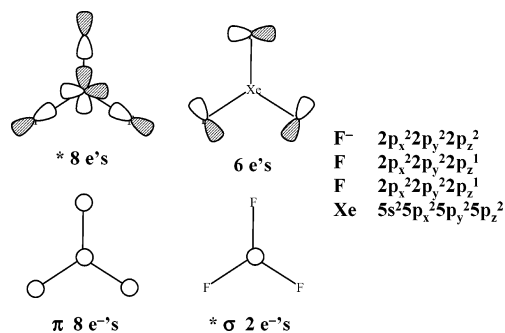
<sup>b</sup> ZPE and thermal energy corrections calculated from the frequencies calculated at the given level of theory, unless otherwise noted. <sup>c</sup> MP4 single-point energies at the MP2 optimized geometry. ZPE and thermal corrections were calculated from frequencies listed in Table 1 and Table S1 in the Supporting Information.

aug-cc-pVTZ level of theory for fluorine. The vibrational frequencies obtained at the other levels of theory are similar. The choice of fluorine basis set does not have a significant effect on the computational results. The enthalpy difference between the Y and T structures ranges from approximately 2 to 15 kJ/mol, and the T structure is found to have a single imaginary frequency at all levels of theory employed. The  $D_{3h}$  triplet is calculated to be a minimum at all levels of theory but is significantly higher in energy than the singlet states. Energies and enthalpies for bonding of fluoride, calculated directly using the energies of Y-shaped  $\text{XeF}_3^-$ ,  $\text{XeF}_2$ , and  $\text{F}^-$ , are listed in Table 2.

## Discussion

Although fluoride does not add to  $\text{XeF}_2$  in solution,<sup>47</sup>  $\text{XeF}_3^-$  can be formed in the gas phase. In order to understand the formation of  $\text{XeF}_3^-$  and its dissociation to form  $\text{XeF}_2$  and  $\text{F}^-$ , it is necessary to understand the electronic structure of  $\text{XeF}_3^-$  itself. The electronic descriptions of systems that disobey the so-called octet rule<sup>48,49</sup> have been somewhat unclear, and various models have been proposed and used.<sup>50</sup> Systems that are electron-deficient have been called “hypovalent”, and Musher has defined “hypervalent” systems as species of Groups 15–18 with 10 or more electrons in the valence shell of the central atom.<sup>51</sup> There have been many approaches for describing the bonding in hypervalent systems. Initially, d-electrons were used to support the concept of an expanded octet, but this notion has been mostly discredited through experimental<sup>25</sup> and computational results.<sup>52</sup> These studies have shown that a three-center, four-electron (3C-4E) bonding model more accurately accounts for the bonding in hypervalent systems<sup>53</sup> such as the trihalide ions.<sup>25,54,55</sup>

There are many different models that could be used to describe the bonding in  $\text{XeF}_3^-$ . Given the large quadrupole

**Figure 2.** Atomic orbitals used for the basis set of  $\text{XeF}_3^-$ . The orbitals marked with an asterisk were used to create the MO diagram in Figure 3.

moment of  $\text{XeF}_2$ , it is tempting to invoke an ion/quadrupole interaction between  $\text{F}^-$  and  $\text{XeF}_2$ . This picture would lead to a T-shaped structure, in agreement with valence-shell electron-pair repulsion (VSEPR) predictions.<sup>56</sup> Indeed, at the B3LYP level of theory, the T structure of  $\text{XeF}_3^-$  is found to be a stationary point on the potential energy surface, with two short Xe–F bonds and one long bond. However, as shown in Table 1, the T-shaped ion is not a stable structure and is calculated to be a transition state ca. 15 kJ/mol higher in energy than a Y-shaped ion, with one short Xe–F bond and two longer Xe–F bonds. Moreover, the measured bond strength of the  $\text{XeF}_2\text{--F}^-$  interaction, 0.84 eV, is much larger than would be predicted for a purely electrostatic ion/quadrupole interaction.<sup>57</sup> In contrast, the  $\text{XeF}_3^+$  ion is known<sup>58–60</sup> to have a stable, near-T structure, consistent with VSEPR predictions for the  $\text{AX}_3\text{E}_2$  structure.<sup>59</sup>

Alternatively, the bonding in  $\text{XeF}_3^-$  can be described by using a molecular orbital approach. Although a simple 3C-4E model is not applicable, the valence molecular orbitals in  $\text{XeF}_3^-$  can be created from a basis set that includes the 5s and 5p orbitals on xenon and the 2p (but not the 2s) orbitals on fluorine, as shown in Figure 2. The relevant symmetry-adapted orbitals of  $\text{XeF}_3^-$ , corresponding to  $D_{3h}$  symmetry, are shown in Figure 3. All of the other electrons, including the  $\pi$  electrons, fully occupy pairs of bonding and antibonding orbitals, and therefore the orbitals do not contribute to the stable electronic structure.

Ten electrons occupy the set of molecular orbitals shown in Figure 3. When using an aufbau approach, the last two electrons are put into an  $e'$  pair of molecular orbitals. With two electrons in two degenerate orbitals,  $D_{3h}$   $\text{XeF}_3^-$  is technically a biradical with four possible electronic states.<sup>61</sup> A Hund's rule approach prefers adding the electrons to the two orbitals with parallel spins to give a triplet state. Three singlet states can be created which correspond to adding both electrons to one of the two orbitals, or adding one to each to create an open-shell singlet state. However, proper description of these states requires multi-configurational wave functions.

On the other hand, the closed-shell singlet states are not stable at high symmetry and undergo second-order Jahn–Teller distortion to lower symmetry  $C_{2v}$  states. The nature of the Jahn–

(47) Brel, V. K.; Zezirov, N. S. Hypervalent Compounds of Xenon. In *Chemistry of Hypervalent Compounds*; Akiba, K.-Y., Ed.; Wiley-VCH: New York, 1999; pp 389.

(48) Langmuir, I. *J. Am. Chem. Soc.* **1919**, *41*, 868.

(49) Lewis, G. N. *J. Am. Chem. Soc.* **1916**, *38*, 762.

(50) Gillespie, R. J.; Silvi, B. *Coord. Chem. Rev.* **2002**, *233–234*, 53.

(51) Musher, J. I. *Angew. Chem., Int. Ed. Engl.* **1969**, *8*, 54.

(52) Reed, A. E.; Schleyer, P. v. R. *J. Am. Chem. Soc.* **1990**, *112*, 1434.

(53) Curnow, O. J. *J. Chem. Educ.* **1998**, *75*, 910.

(54) Nizzi, K. E.; Pommerening, C. A.; Sunderlin, L. S. *J. Phys. Chem. A* **1998**, *102*, 7674.

(55) Sunderlin, L. S. *Adv. Gas Phase Ion Chem.* **2001**, *4*, 49.

(56) Liebman, J. F. *J. Fluorine Chem.* **1976**, *7*, 531.

(57) Calculated to be 0.25 eV by using the quadrupole moment of  $\text{XeF}_2$  obtained from electronic structure calculations at the optimized geometry of the T-shaped structure.

(58) McKee, D. E.; Adams, C. J.; Zalkin, A.; Bartlett, N. J. *Chem. Soc., Chem. Commun.* **1973**, 26.

(59) McKee, D. E.; Zalkin, A.; Bartlett, N. *Inorg. Chem.* **1973**, *12*, 1713.

(60) Boldrin, P.; Gillespie, R. J.; Ireland, P. R.; Schrobilgen, G. J. *Inorg. Chem.* **1974**, *13*, 1690.

(61) Salem, L.; Rowland, C. *Angew. Chem., Int. Ed.* **1972**, *11*, 92.

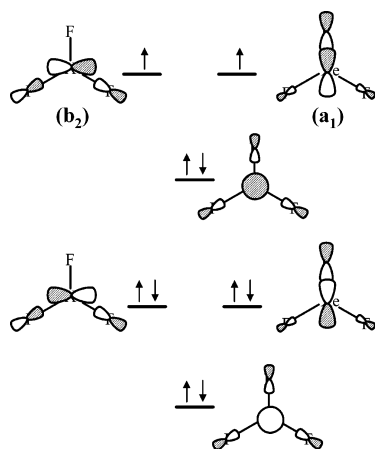


**Figure 3.** Simplified symmetry-adapted frontier molecular orbitals of  $\text{XeF}_3^-$  derived from the basis atomic orbitals shown in Figure 2. The symmetry labels for the two singly occupied orbitals correspond to  $C_{2v}$  symmetry.

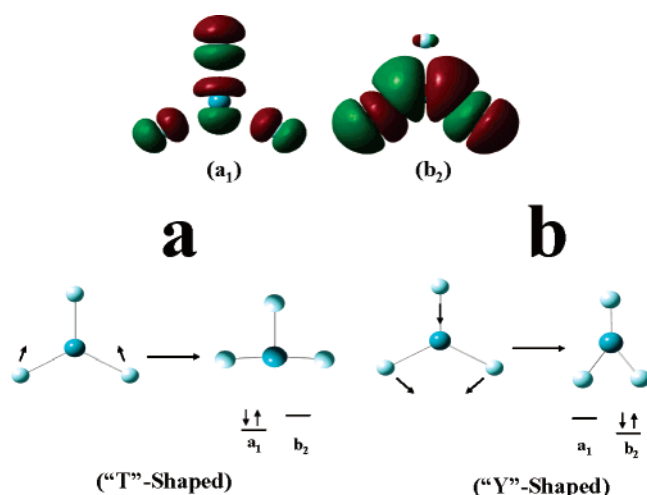
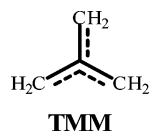


**Figure 4.** Coordinates for the Jahn-Teller distortions from  $D_{3h}$  to the (a) T-shaped and (b) Y-shaped structures of  $\text{XeF}_3^-$ , along with the effect on the relative orbital energies. Symmetry labels refer to the  $C_{2v}$  descriptions.

Teller distortions is shown in Figure 4. The  $e'$  pair of orbitals in  $D_{3h}$  symmetry reduce to  $a_1$  and  $b_2$  symmetry types in  $C_{2v}$  and are shown at the top of Figure 4. The Jahn-Teller distortions that occur are shown at the bottom of the figure. Distortion of the molecule as shown in Figure 4a decreases the antibonding interaction in the  $a_1$  orbital, lowering its energy. The resulting geometry is that of the T-shaped ion, with an electronic structure  $a_1^2 b_2^0$ . Alternatively, distorting the molecule as in Figure 4b destabilizes the  $a_1$  orbital. The resulting geometry is the Y-shaped structure, with an electronic structure  $b_2^2 a_1^0$ . Thus, by this molecular orbital picture, it can be seen that the T-shaped and Y-shaped structures of  $\text{XeF}_3^-$  constitute a Jahn-Teller pair of states originating from the same  $D_{3h}$  ion. The Jahn-Teller distortion significantly stabilizes the  $\text{XeF}_3^-$  ion, as the triplet state is found to be ca. 60–110 kJ/mol higher in energy than the ground state (Table 1).

In many ways, the electronic structure of  $\text{XeF}_3^-$  resembles that of the trimethylenemethane diradical (TMM). Like  $\text{XeF}_3^-$ ,



TMM

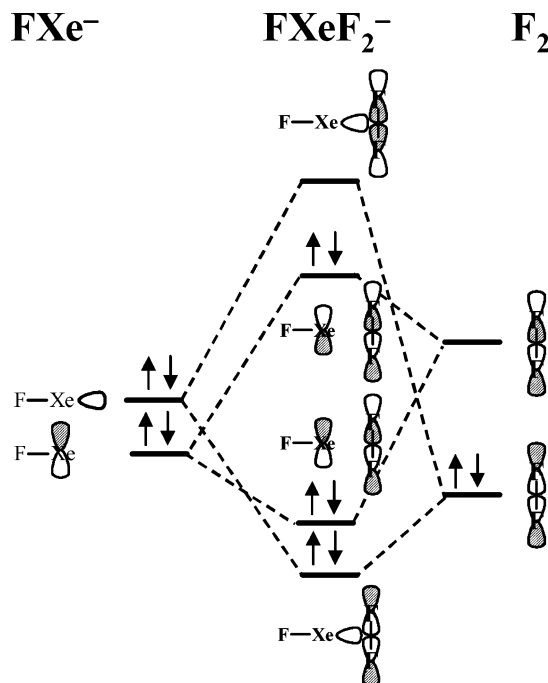


**Figure 5.** Simple molecular orbital diagram describing the electronic structure of the Y-shaped  $\text{XeF}_3^-$  structure as interactions between  $\text{FXe}^-$  and  $\text{F}_2$ . Alternatively, a similar diagram could be constructed for the interaction of  $\text{XeF}^+$  with  $\text{F}_2^{2-}$  by moving two electrons from  $\text{XeF}$  to the antibonding orbital of  $\text{F}_2$ .

TMM has two electrons that occupy a degenerate pair of orbitals at the  $D_{3h}$  geometry.<sup>62–65</sup> Moreover, the singlet states of TMM undergo Jahn-Teller distortion to two lower-symmetry,  $C_{2v}$  structures by the same type of motions that are shown in Figure 4.<sup>66</sup> Therefore,  $\text{XeF}_3^-$  has characteristics that resemble those of traditional diradicals, although the extent of diradical character in  $\text{XeF}_3^-$  is not large in the  $C_{2v}$  geometries.<sup>67</sup>

Molecular orbital (MO) descriptions of the Y and T structures of  $\text{XeF}_3^-$  can also be constructed by considering the interactions of different components. For example, as shown in Figure 5, the bonding in the Y-shaped structure results from two interactions between  $\text{XeF}^-$  and  $\text{F}_2$ . Orbitals that resemble  $\sigma$  and  $\sigma^*$  are formed by interaction of the occupied  $\sigma$  orbital in  $\text{XeF}^-$  with the  $\sigma$  orbital in  $\text{F}_2$ , whereas  $\pi$ -type orbitals are created from the 5p orbital on Xe with the  $\sigma^*$  orbital in  $\text{F}_2$ . A similar MO picture for the Y-shaped geometry would result by considering the interaction of  $\text{XeF}^+$  with  $\text{F}_2^{2-}$ . Conversely, the orbitals in the T-shaped structure resemble those that arise from interaction between fluoride ion and  $\text{XeF}_2$ , as shown in Figure 6. The relevant orbitals on  $\text{XeF}_2$  are the nonbonding and antibonding combinations of p orbitals used to create the 3C-4E bond.<sup>55,68</sup>

Electronic structure calculations predict the Y-shaped structure of  $\text{XeF}_3^-$  to be bound by about 1 eV with respect to formation of fluoride and linear  $\text{XeF}_2$  (Table 2), in good agreement with the measured value of 0.84 eV. However, attempts to calculate

(62) Yarkony, D. R.; Schaefer, H. F., III. *J. Am. Chem. Soc.* **1974**, *96*, 3574.

(63) Borden, W. T.; Davidson, E. R. *J. Am. Chem. Soc.* **1977**, *99*, 4587.

(64) Cramer, C. J.; Smith, B. *J. Phys. Chem.* **1996**, *100*, 9664.

(65) Slipchenko, L. V.; Krylov, A. I. *J. Chem. Phys.* **2003**, *118*, 6874.

(66) Davidson, E. R.; Borden, W. T. *J. Am. Chem. Soc.* **1977**, *99*, 2053.

(67) The ratio of CI coefficients in a two-configuration self-consistent field calculation at the optimized Y geometry is 6.7, indicating a wave function that is approximately 2% diradical.

(68) Pimentel, G. C. *J. Chem. Phys.* **1951**, *19*, 446.

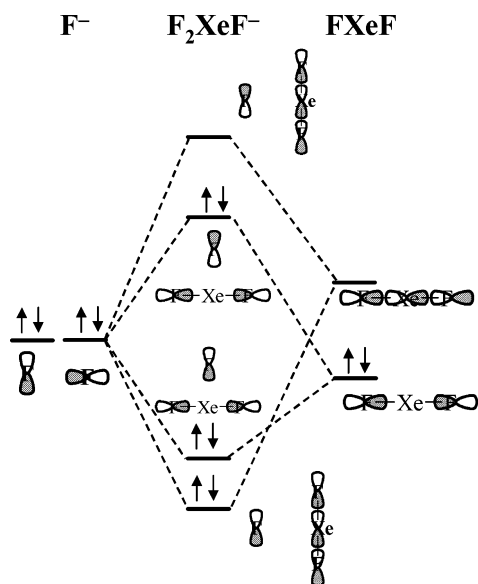


**Figure 6.** Simple molecular orbital diagram describing the electronic structure of the T-shaped  $\text{XeF}_3^-$  structure as interactions between  $\text{F}^-$  and  $\text{XeF}_2$ .

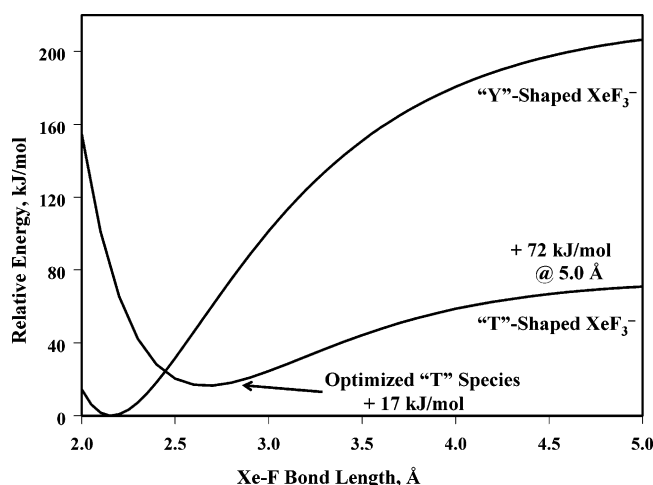


**Figure 7.** Plots of electronic energy vs Xe–F distance for loss of fluoride from Y-shaped and T-shaped  $\text{XeF}_3^-$ , under the constraint of  $C_{2v}$  symmetry. Calculated by using the B3LYP approach with the Maroulis basis set<sup>40</sup> for xenon and the 6-31+G\* basis set for fluorine.

the energy profile for direct  $\text{F}^-$  loss from Y-shaped  $\text{XeF}_3^-$  under the constraints of  $C_{2v}$  symmetry lead to an asymptotic value of more than 200 kJ/mol (Figure 7). In contrast, direct loss of fluoride from the T-shaped structure proceeds without a barrier in excess of the endothermicity. The high barrier for direct fluoride loss from the Y-shaped ion results because the Y-shaped ion correlates electronically with an excited state of  $\text{XeF}_2$  upon loss of fluoride. The MO diagram in Figure 5 shows that Y-shaped ion correlates with  $\text{XeF}^-$  and  $\text{F}_2$  products, whereas it is the T-shaped ion that correlates with ground-state  $\text{XeF}_2 + \text{F}^-$ . Therefore, in order for adiabatic dissociation to occur, the Y-shaped ion first needs to rearrange to a T-shaped structure that can dissociate directly.

A more detailed description of the dissociation pathways requires consideration of multiple dimensions. A contour plot of the energy of singlet  $\text{XeF}_3^-$  as a function of two dimensions is shown in Figure 8. The coordinates of the plot are two F–Xe–F bond angles. The system is restricted to planarity,

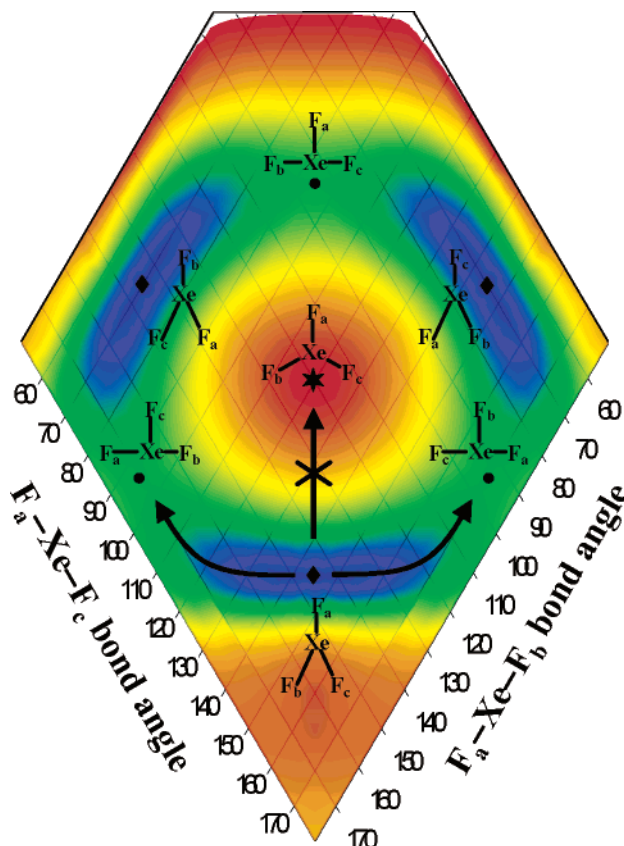


**Figure 8.** Contour plot of the electronic energies of singlet  $\text{XeF}_3^-$  as a function of F–Xe–F bond angles. The calculation was carried out using the B3LYP approach, using the SDB-cc-pVTZ basis set for xenon and a 6-31+G\* basis set for fluorine. The Xe–F bond distances were optimized at each point. Low-energy regions are indicated in blue, and the high-energy regions are in red. Positions of the Y, T, and  $D_{3h}$  structures are indicated, and the relative enthalpies for the Y and T structures are listed in Table 1. The arrows indicate the paths for pseudorotation leading to interconversion of the Y structures.

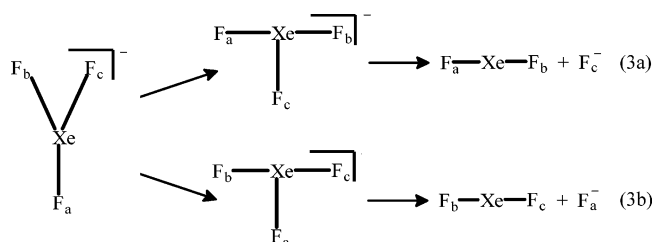
with the third bond angle determined by the other two, and the bond lengths are optimized at each set of bond angles. The energies are the electronic energies calculated using the B3LYP approach with the SDB-cc-pVTZ basis set for Xe and a 6-31+G\* basis set for fluorine. The threefold degeneracy of the  $\text{XeF}_3^-$  ion is apparent in the plot, as there are three equivalent versions of the Y-shaped ion (indicated by the diamond in the dark blue section), at approximate bond angles (70,145), (145,70), and (145,145). The positions of the T structures are indicated by the circles in the green area near (95,170), (170,95), and (95,95). The  $D_{3h}$  structure is at the point (120,120) and is indicated by a star. The fact that the  $D_{3h}$  structure is in the red section of the plot reflects the high energy of this point.<sup>69</sup> The surface of  $\text{XeF}_3^-$  is similar to that described in detail previously for singlet trimethylenemethane.<sup>66</sup>

The contour plot provides additional insight into the dissociation process. As noted above, adiabatic dissociation requires rearrangement from the Y-shaped to the T-shaped ion. The contour plot shows that this process occurs via a pseudorotation, and not by direct (symmetry-retaining) transformation. Thus, the Y-shaped ion in which  $\text{F}_b$  and  $\text{F}_c$  are equivalent (near the

(69) Because calculation of the  $D_{3h}$  singlet requires a multi-configurational approach, the energy at that geometry was not calculated directly but was estimated from points near it.



bottom center of Figure 8) preferably rearranges to a T-shaped structure in which  $F_b$  and  $F_c$  are distinct (bottom right or bottom left), and either  $F_b$  (right) or  $F_c$  (left) is lost in the dissociation (eq 3a). On the other hand, simple flattening of the Y to the T



structure (eq 3b) requires passing through the  $D_{3h}$  point at much higher energy. Loss of a fluoride from one of the “arms” of the Y structure is the simplest low-energy dissociation pathway, whereas loss of the fluoride from the base requires rearrangement to an alternate Y structure if it is to occur at the reaction threshold. After collisional activation, any ion with sufficient energy to dissociate has sufficient energy to access all three forms of the Y-geometry.

Whereas bonding is normally considered from the perspective of the energy lowering of filled orbitals, it can also be considered as the energy raising of empty (or half-empty) ones. A normal single bond, from this perspective, reflects the rise in energy of the unoccupied antibonding orbital (i.e., two electron holes).  $XeF_2$  and  $XeF_3^-$  also have two electron holes, giving a nominal bond order of 1. However, a hypervalent 3C-4E bonded system like  $XeF_2$  is stable because the unfilled orbital (the top right orbital in Figure 6) is more unstable than a two-center antibonding orbital. Overall, the MO diagrams in Figures 5 and 6 indicate that singlet  $XeF_3^-$  has an overall bond order of 1. In contrast,  $XeF_3^+$ , which contains two fewer electrons, has a bond order of 2, which likely accounts for why  $XeF_3^+$  is more stable and can be formed in a crystalline state.<sup>58–60</sup> The  $D_{3h}$  structure of  $XeF_3^-$  is about as stable as the unbound pair,  $XeF_2 + F^-$ , because the two electron holes in this species, as shown in Figure 3, reside in orbitals that are about as antibonding as the unfilled 3C-4E orbital. The Jahn–Teller distortion shown in Figure 4 raises the two electron holes to higher energy, corresponding to a lowering of energy of filled orbitals that gives rise to the observed binding energy in  $XeF_3^-$ . Thus, it is the Jahn–Teller distortion that makes  $XeF_3^-$  a stable species in the gas phase.

The bond dissociation energy of  $XeF_3^-$  is likely much stronger in the gas phase than it is in solution due to the differences in solvation energies of the ion and  $F^-$ . In a recent study of the bonding in  $F_3^-$ , it was estimated that the difference

between the solvation energies ( $\Delta G_{solv}$ ) of  $F_3^-$  and the dissociation products,  $F^- + F_2$ , is 150 kJ/mol.<sup>25</sup> Given that  $XeF_3^-$  is larger than  $F_3^-$ , the Born model would predict that the solvation energy difference should be larger as well. Therefore,  $XeF_3^-$  would not be expected to be stable with respect to dissociation in aqueous solution.

## Conclusion

The bond dissociation energy in  $XeF_3^-$  reported in this study indicates a mode of bonding that is stronger than what is expected for electrostatic interactions or simple 3C-4E bonding. The bonding in  $XeF_3^-$  is described by using two different molecular orbital approaches. One approach, using symmetry-adapted molecular orbitals, results in a diradical-like model for  $XeF_3^-$ . Jahn–Teller distortion leads to the formation of low-energy singlet states with Y and T geometries. The diradical approach also accounts for the presence of a higher-energy triplet state of the ion. A second MO approach utilizes orbital interactions between different components of the ion. The ground-state, Y-shaped ion is described as an interaction between the occupied orbitals on  $XeF^-$  and the empty, antibonding ( $\sigma^*$ ) orbital on  $F_2$ , whereas the T-shaped structure is described as an interaction between  $F^-$  and the 3C-4E bonding orbitals in  $XeF_2$ . The orbital interaction approach also provides a correlation diagram for the dissociation of  $XeF_3^-$ , indicating that direct (symmetry-retaining) dissociation of  $F^-$  to form the ground state of  $XeF_2$  can occur only for the T-shaped ion. Surface calculations indicate that the Y-shaped ion can rearrange to the T structure by pseudorotation around but not through the  $D_{3h}$  geometry.

**Acknowledgment.** Support for this work was provided by the National Science Foundation (CHE04-54874, P.G.W.; CHE99-85883, L.S.S.). We thank Profs. Peter Armentrout, Mary Rodgers, and Kent Ervin for use of the CRUNCH software for data analysis, and Anna Krylov for discussions regarding the properties of TMM.

**Supporting Information Available:** Complete refs 35 and 36, and computed bond lengths for  $XeF_2$ . This material is available free of charge via the Internet at <http://pubs.acs.org>.

JA065038B